Nanoparticle-tuned structural color from polymer opals

Otto L. J. Pursiainen[1], Jeremy J. Baumberg[1*], Holger Winkler[2], Benjamin Viel[3], Peter Spahn[3],and Tilmann Ruhl[3]

[1]*School of Physics and Astronomy, University of Southampton, Highfield, Southampton, SO17 1BJ, United Kingdom*
[2] *Merck KGaA, Frankfurter Strasse 250, D-64291 Darmstadt, Germany*
[3]*Deutsches Kunststoff-Institut (DKI), Schlossgartenstrasse 6, D-64289 Darmstadt, Germany*
j.j.baumberg@soton.ac.uk

Abstract: The production of high-quality low-defect single-domain flexible polymer opals which possess fundamental photonic bandgaps tuneable across the visible and near-infrared regions is demonstrated in an industrially-scalable process. Incorporating sub-50nm nanoparticles into the interstices of the *fcc* lattice dramatically changes the perceived color without affecting the lattice quality. Contrary to iridescence based on Bragg diffraction, color generation arises through spectrally-resonant scattering inside the 3D photonic crystal. Viewing angles widen beyond 40º removing the strong dependence of the perceived color on the position of light sources, greatly enhancing the color appearance. This opens up a range of decorative, sensing, security and photonic applications, and suggests an origin for structural colors in Nature.

OCIS codes: (999.9999) Photonic crystals, (330.1690) Color, (160.4760) Optical properties, (290.5850) Scattering, particles, (160.5470) Polymers

References and links

1. R. K. Iler, "Formation of precious opal," Nature **207**, 472-473 (1965).
2. P. J. Darragh, A. J. Gaskin, B. C. Terrell, and J. V. Sanders, "Origin of precious opal," Nature **209**, 13-16 (1966).
3. J. V. Sanders and M. J. Murray, "Ordered arrangements of spheres of two different sizes in opal," Nature **275**, 201-203 (1978).
4. A. van Blaaderen, "Opals in a new light," Science **282**, 887-888 (1998).
5. D. W. Oxtoby, "Crystallization: Diversity suppresses growth," Nature **413**, 694-695 (2001).
6. P. Vukusic and J. R. Sambles, "Photonic structures in biology," Nature **424**, 852-855 (2003).
7. H. Ghiradella, D. Aneshansley, T. Eisner, R. E. Silberglied, and H. E. Hinton, "Ultraviolet reflection of a male butterfly: Interference color caused by thin-layer elaboration of wing scales," Science **178**, 1214-1217 (1972).
8. A. Jenkins, "Photonics: Wingèd light," Nature **438**, 436 (2005).
9. P. Vukusic and I. Hooper, "Directionally controlled fluorescence emission in butterflies," Science **18**, 1151 (2005).
10. E. Yablonovitch, "Inhibited spontaneous emission in solid-state physics and electronics," Phys. Rev. Lett. **58**, 2059-2062 (1987).
11. S. John, "Strong localization of photons in certain disordered dielectric superlattices," Phys. Rev. Lett. **58**, 2486-2489 (1987).
12. J. E. G. J. Wijnhoven and W. L. Vos, "Preparation of photonic crystals made of air spheres in titania," Science **281**, 802-804 (1998).
13. R. de la Rue, "Photonic crystals: Microassembly in 3D," Nature Mater. **2**, 74–76 (2003).
14. P. V. Braun and P. Wiltzius, "Electrochemically grown photonic crystals," Nature **402**, 603-604 (1999).
15. G. Subramania, K. Constant, R. Biswas, M. M. Sigalas, and K. -M. Ho, "Inverse face-centered cubic thin film photonic crystals," Adv. Mater. **13**, 443-446 (2001).
16. A. A. Zakhidov, R. H. Baughman, Z. Iqbal, C. Cui, I. Khayrullin, S. O. Dantas, J. Marti, and V. G. Ralchenko, "Carbon structures with three-dimensional periodicity at optical wavelengths," Science **282**, 897-901 (1998).
17. J. H. Holtz and S. A. Asher, "Polymerized colloidal crystal hydrogel films as intelligent chemical sensing materials," Nature **389**, 829-832 (1997).

#82645 - $15.00 USD Received 1 May 2007; revised 4 Jul 2007; accepted 9 Jul 2007; published 17 Jul 2007

18. A. C. Arsenault, T. J. Clark, G. von Freymann, L. Cademartiri, R. Sapienza, J. Bertolotti, E. Vekris, S. Wong, V. Kitaev, I. Manners, R. Z. Wang, S. John, D. Wiersma, G. A. Ozin, J. M. Jethmalani, and W. T. Ford, "Diffraction of visible light by ordered monodisperse silica-poly(methyl acrylate) composite films," Chem. Mater., **8**, 2138-2146 (1996).
19. S. H. Foulger, P. Jiang, A. Lattam, D. W. Smith Jr., J. Ballato, D. E. Dausch, S. Grego, and B. R. Stoner, "Photonic crystal composites with reversible high-frequency stop band shifts," Adv. Mater. **15**, 685-689 (2003).
20. T. Ruhl, P. Spahn, and G. P. Hellmann, "Artificial opals prepared by melt compression," Polymer **44**, 7625-7634 (2003).
21. O. L. J. Pursiainen, J. J. Baumberg, H. Winkler, B. Viel, and T. Ruhl, "Compact strain-sensitive flexible photonic crystals for sensors," Appl. Phys. Lett. **87**, 101902-101904 (2005).
22. G. Labeyrie, C. A. Muller, D. S. Wiersma, C. Miniatura, and R. Kaiser, "Observation of coherent backscattering of light by cold atoms," J. Opt. B: Quantum Semiclass. Opt. **2**, 672–685 (2000).
23. Using conventional spectro-photometers thus yields erroneous measurements as some significant fraction of S is also collected.
24. V. N. Astratov, A. M. Adawi, S. Fricker, M. S. Skolnick, D. M. Whittaker, and P. N. Pusey "Interplay of order and disorder in the optical properties of opal photonic crystals," Phys. Rev. B **66**, 165215-165227 (2002).
25. T. Ruhl and G. P. Hellmann, "Colloidal crystals in latex films: rubbery opals," Macromol. Chem. Phys. **202**, 3502-3505 (2001).
26. Yu. A. Vlasov, M. A. Kaliteevski, and V. V. Nikolaev, "Different regimes of light localization in a disordered photonic crystal," Phys. Rev. B **60**, 1555-1562 (1999).
27. R. Rengarajan, D. Mittleman, C. Rich, and V. Colvin, "Effect of disorder on the optical properties of colloidal crystals," Phys. Rev. E **71**, 016615-016625 (2005).
28. A. F. Koenderink and W. L. Vos, "Optical properties of real photonic crystals: anomalous diffuse transmission," J. Opt. Soc. Am. B **22**, 1075-1084 (2005).
29. C. Hermann and O. Hess, "Modified spontaneous-emission rate in an inverted-opal structure with complete photonic bandgap," J. Opt. Soc. Am. B **19**, 3013-3018 (2002).
30. R. C. McPhedran, L. C. Botten, J. McOrist, A. A. Asatryan, C. M. de Sterke, and N. A. Nicorovici, "Density of states functions for photonic crystals," Phys. Rev. E **69**, 16609-16624 (2004).
31. A. V. Baryshev, V. A. Kosobukin, K. B. Samusev, D. E. Usvyat, and M. F. Limonov, "Light diffraction from opal-based photonic crystals with growth-induced disorder: Experiment and theory," Phys. Rev. E**73**, 205118 (2006).
32. S. A. Asher, J. M. Weissman, A. Tikhonov, R. D. Coalson, and R. Kesavamoorthy, "Diffraction in crystalline colloidal-array photonic crystals," Phys. Rev. B**69**, 066619 (2004).

1. Introduction

Structural color in nature arises mostly from optical interference of multiple light paths reflected inside periodically-textured materials. Natural opals consisting of stacked silica spheres acquire their characteristic iridescence due to Bragg interference from the lattice planes [1-6]. Similarly butterfly wings can change their color with viewing angle due to the grating-like fine structure on their surfaces [6-9].

Photonic crystals have attracted great interest since initial proposals suggested the inhibition of light emission in periodic structures [10-11]. Formation of complete photonic band gaps requires large refractive index contrast between the different components. Recently, there has been great interest in fabricating artificial opals or inverse opal structures [12-16] as their structural color can replace toxic and carcinogenic dyes. However, the problem with these structures is their poor lattice quality due to cracks and poly-crystallinity, and their rigidity, which limits practical structural color applications.

Here we present here an alternative but *industrially-scalable* approach that produces low contrast flexible opals from polymers for structural color applications. In contrast to previous methods for producing flexible opals [17-19], large-scale structural assembly is directed by the shear-flow alignment of core-shell nano-spheres in a polymer melt. This process additionally allows the localized doping of these opals by incorporation of nanoparticles, which is difficult to achieve in other fabrication procedures. Such nanoparticle doping allows the color hue and directionality to be tailored, despite the low relative refractive index contrast between the polymeric components. These crystals exhibit color features not explained by any conventional Bragg diffraction scheme, which is the normal mechanism invoked for the structural colors of butterfly wings, iridescent beetles or natural opals. Instead, they rely on a

#82645 - $15.00 USD Received 1 May 2007; revised 4 Jul 2007; accepted 9 Jul 2007; published 17 Jul 2007

new color generation phenomenon arising from resonant scattering events that take place inside the structured environment of the photonic crystal.

Our ability to compression mould these flexible films, and to create emissive quantum-dot-doped polymer opals, anticipates their use in a range of decorative, sensing, security and photonic applications. Our results also suggest a re-examination of structural color in nature which we believe may exploit the same phenomena.

2. Opal fabrication

Our fabrication technique exploits polymer nano-sphere interactions in the viscous melt when lateral shear forces are applied, either by transverse pressure, or through extrusion [20]. These sub-micron particle precursors have a core-shell architecture consisting of a hard crosslinked polystyrene (PS) sphere coated with a thin polymethyl-methacrylate (PMMA) inter-layer which anchors the outer shell composed of soft polyethylacrylate (PEA). During shear flow [Fig. 1(a)], these core particles self-assemble into an *fcc*-lattice with the soft PEA shell filling the interstitial voids [20]. The fundamental optical response arising from the Bragg reflections (or incomplete photonic bandgaps) can be directly tuned across the visible and near-infrared spectral regions by varying the precursor nano-sphere size (around 200-350nm), and hence the resulting lattice parameter. The thickness of these thin opals can be straightforwardly varied between 100-300 μm. One of the most attractive features is the flexibility and the malleability of these structures, with color highlights produced by the bending or stretching modification of the (111) plane spacing [21].

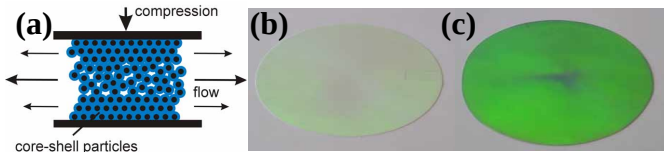

Fig. 1. (a). Compression shear-assembly of polymer opal. (b-c) Optical images under natural lighting of 10cm diameter polymer opal films, which are (b) undoped (**S3**) and (c) doped (**S4**) with 0.05% by weight carbon nanoparticles.

Critical for the work here, is the ability to introduce additional sub-50nm nanoparticle dopants into the interstices of the photonic crystal lattice without disrupting the lattice quality. This is achieved by introducing the nanoparticle dopants into the precursor mix resulting in their homogeneous distribution within the interstitial PEA voids. A detailed description of the manufacturing can be found in Ref. [20]. The nanoparticle dopant we concentrate on in the present paper is carbon, however we have also successfully incorporated gold and hematite nanoparticles as well as CdSe colloidal quantum dots to produce emissive films. Results here are taken on 15cm-diameter polymer opal sheets produced by polymer melt compression, which we have shown previously are representative of the process, and can be well controlled. Samples studied in this work vary in precursor sphere size and different carbon black nanoparticle concentration (Table 1).

The key result we concentrate on here is that by introducing only 0.05% (by weight) of carbon nanoparticles into the lattice structure, the visual appearance of the elastomeric opals changes quite remarkably from milky white to intense green [Figs. 1(b)-1(c)]. These pictures are taken under natural lighting conditions and show the weak and highly-orientation-dependent Bragg diffraction gives way to a new color mechanism which is relatively insensitive to viewing angle. Detailed measurements of the angular optical response below strongly indicate that this effect is due to resonant scattering inside the photonically-structured environment and is critically dependent on the use of low-, not high-, refractive-index-contrast photonic crystals.

#82645 - $15.00 USD Received 1 May 2007; revised 4 Jul 2007; accepted 9 Jul 2007; published 17 Jul 2007

Table 1. Structural and doping parameters for several polymer opal films used in this work.

Sample	sphere diameter (nm)	normal incidence (111) bandgap (nm)	carbon nanoparticle concentration (wt-%)
S1	250	635	0.20
S2	354	901	0.10
S3	236	601	0.00
S4	236	601	0.05
S5	236	601	0.10
S6	236	601	0.20

We confirm that the introduction of the nanoparticle doping at such low concentrations does not affect the structural quality of the opaline films, using a number of techniques. A large number of cross-sections examined by transmission electron microscopy (TEM) *in every case* show excellent lattice ordering in the hundreds of layers that light penetrates from the top of the films. Both with and without doping, this lattice uniformity is preserved [Figs. 2(a)-2(b)], with up to 30% loading of each interstice in the lattice with a carbon nanoparticle. Note that shear in the TEM images is produced in the microtoming of the relatively soft films. This excellent surface-ordering quality can also be verified from the six-fold *surface* diffraction pattern observed *across the entire sample* [Fig. 2(b) inset], taken with a 244nm UV laser normally incident on sample **S2** with the diffracted UV light observed on a fluorescent white card. The penetration of UV light is on the order of a few hundred nanometers in these polymers (due to UV absorption in the polymer mix) and hence only surface ordering can be probed. Further confirmation of the single domain nature of the opal fabrication is seen [Fig. 2(c)] when comparing the Bragg diffraction from the poly-crystals of typical high-quality sedimented opal (left) with that from the mono-domain composing the opaline film (right, note that the gradation in color is because the flexible opal is intentionally bent).

These structural colors can be readily incorporated into applications, for instance in compression moulding onto an automobile model [Fig. 2(d)] producing highlighted color changes on the edges. We have produced >100m lengths of such extruded polymer opals showing the capability for industrial scalability.

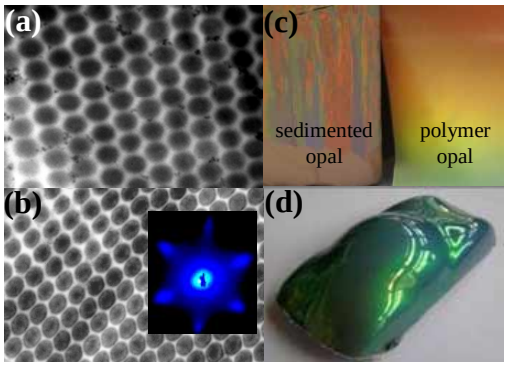

Fig. 2. (a).-(b). TEM images of the (111) lattice plane of sample **S4**, where the polymer in (b) has been stained with ruthenium tetroxide for better contrast of the polystyrene/polyacrylate system. Inset of (b): surface diffraction pattern of sample **S2** under normal incidence UV illumination. (c) Digital images of a sedimented and a polymer opal **S1**. (d) Miniature automobile with moulded polymer opal.

3. Experimental setups

The angle dependence of the Bragg-reflection and scattering was studied in two different setups. In the goniometer setup [Fig. 3(a)] the sample was mounted on a rotation stage and

#82645 - $15.00 USD Received 1 May 2007; revised 4 Jul 2007; accepted 9 Jul 2007; published 17 Jul 2007

excited by an unpolarised super-continuum light source (emitted by a holey fiber pumped with 1064nm Nd-YAG microchip laser pulses) focused to a 500μm spot. On the detection arm are two lenses (L1 to collimate reflected/scattered light and L2 to refocus it on a multimode fiber) and in between is a variable-diameter iris. In the experiments reported here we fix the detection angle at the mirror reflection angle ($\theta_r=\theta_i$), but vary the iris aperture to record the strictly reflected (*R*) light (collection angle $\Delta\theta_r$=3° equal to the input laser collimation) or the wide-angle-scattered (*S*) contribution (iris fully open, collection angle $\Delta\theta_s$=30°). The light was then focussed into a multimode fiber (200μm core) which was coupled to an Ocean Optics USB2000 spectrometer. We separately confirmed that the phenomena presented here are not significantly dependent on input and output polarization.

To map a wider angular scattering cone we use a hyperspectral imaging setup [Fig. 3(b)]. Here the incident light from the super-continuum source is first spectrally filtered (tunable center wavelength 400-700nm with a 7-nm bandwidth) using a CRI Varispec filter, and the incident light is *p*-polarised. For fixed incident angle, at each incident wavelength we record the resulting reflection/scattering (*R/S*) emission on a semi-transparent hemi-spherical white screen centered at the sample focus, using a zoom lens and CCD-camera which are aligned along the axis of the specular reflection angle. The spectral response is calibrated by replacing the sample with an aluminum mirror and recording the directly reflected spectrally-filtered laser [which appears as a small spot in the center of the images - see white spot in center of Fig. 4(b)]. Knowledge of the imaging geometry enables us to extract from the images obtained for each sample the angular widths of the different scattering cones at each wavelength [Figs. 4(c), 5(d), 6(d)]. The experiment is repeated at different angles of incidence to identify scattering that depends on the direction of incoming light (ie. identifying scattering with some memory of incident **k** orientation). For illustrative purposes, the full scattering is recorded on a white screen in Fig. 4(b) using a color digital camera in the geometry depicted in Fig. 4(a).

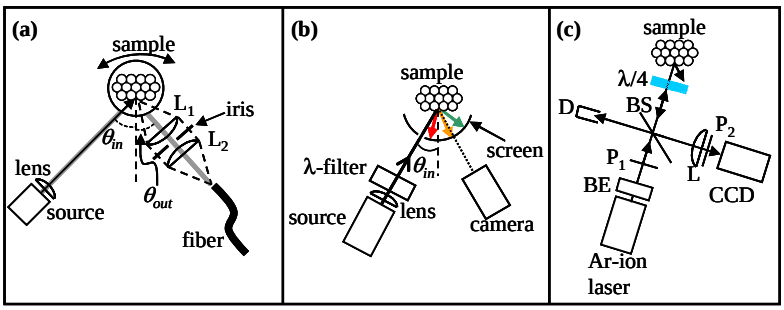

Fig. 3. Experimental setups used for (a,b) angle-dependent reflectivity and scattering measurements, (c) coherent backscattering mean free path measurements.

In order to quantify the effect of nanoparticle doping, the scattering mean free paths (l_{mfp}) are measured using a standard coherent back-scattering (CBS) technique [22]. Here [Fig. 3(c)], the light from an Ar^+ laser at 514.5nm is beam expanded six-fold (BE) to 10mm diameter, vertically polarized (P1) and incident on a beamsplitter (BS). While the reflected component of the beam is carefully beam-dumped (D), the transmitted beam passes through a λ/4 waveplate to change its polarization state into right-circular (σ+) before being incident on the sample. Since the multiply-scattered light does not flip its polarization [22], after direct backscatter ($\theta_{CBS}=-\theta_i$) the emerging light is converted back into vertical polarization (by the λ/4) and reflected off the BS into the CCD camera. With the polarizer P2 set vertically, only multiply-scattered contributions are transmitted while singly-scattered photons which emerge with left-circular (σ–) polarization are subsequently rejected by P2. The 150mm focusing lens (L) converts different back-scatter angles into spatial position in the image, which is

#82645 - $15.00 USD Received 1 May 2007; revised 4 Jul 2007; accepted 9 Jul 2007; published 17 Jul 2007

calibrated from the geometry. The mean free paths were then calculated from the (~mrad) angular width of the coherent back-scattering peak using Ref. [22].

4. Results and discussion

The peculiar optical properties of these polymer opals arise from chromatically-redirected scattering. To first demonstrate this we use a simple imaging geometry [Fig. 4(a)] in which light from a white light laser continuum source is incident at an angle of 40º on sample **S1** and the resulting scattered light emerging from the opal around the reflection angle is recorded using a digital camera [Fig. 4(b)]. The chromatic scattering shows different colors emerging in different directions surrounding the central white reflected laser spot (*R*). By spectrally filtering the incident laser as described in Fig. 3(a), we image the evolution of the scattering cone across the photonic bandgap, centered here at 580nm [Fig. 4(c)]. The superimposed white dashed lines intersect in the specular reflected direction (reflected spot divergence ~3º), and strong scattering is seen over 30º away from this specular reflection angle.

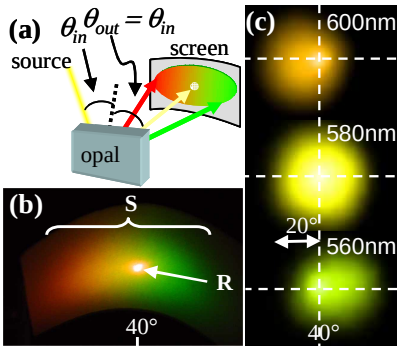

Fig. 4. (a). Scattering geometry employed. (b). Optical image of the front surface scattering of the polymer opal **S1** revealing the structural color content, light incident and reflected at 40º. (c) Scattering cone of **S1** for three different color components at, and on the red and blue sides of the bandgap at 580nm for 40° incidence. Specular reflected spot at intersection of lines.

To demonstrate the influence of Bragg scattering within the photonic crystal, the full reflection of light including the scattering component is measured as a function of the size of the sphere precursor used to make the opal samples [Fig. 5(a)]. A strong peak is observed, which tunes proportional to sphere separation according to the standard Bragg equation for (111) planes parallel to the front surface. The relationship between reflection and scattering is then extracted from angle-dependent spectra in which either the full scattering intensity (*R*+*S*), or only the reflected contribution in the central spot (*R*), is measured [Fig. 5(b)]. In this experimental configuration [Fig. 3(a)] the light emerging from the sample is collected within an angular cone whose width is controllable, and focused into a multimode fiber connected to a spectrometer. The full scattering intensity (red line, 30º collection angular width) peaks at the expected Bragg spectral position for this angle of incidence. However when only the reflected spot is collected (3º cone angle, black line), a deep dip is observed [23]. By subtracting these two, the scattered contribution is identified (blue line) which exhibits a strong resonant peak. Comparing the contrast on- and off-resonance, for reflection this ratio is <0.2 (the residual measured on resonance is also probably scatter – see below) while for scattering this ratio is >15. Counter to the conventional picture for photonic crystals of enhanced reflectivity at the Bragg resonance, we observe almost *no* light reflected in this Bragg condition. Simultaneously we observe strongly-enhanced scattering maximized near the same spectral position. Light entering the sample at the band gap wavelength is almost all redistributed into a wide scattering cone around the reflection direction.

To confirm that this scattering is dependent on the Bragg resonance, extraction of *R* and *S* is carried out for different angles of incidence [Fig. 5(c)]. Both the scattering peak and the

#82645 - $15.00 USD Received 1 May 2007; revised 4 Jul 2007; accepted 9 Jul 2007; published 17 Jul 2007

reflection dip tune exactly in accordance with the (111)-plane Bragg resonance expected for the periodicity of this sample [Fig. 5(c) inset shows theoretical line with experimental points].

This phenomenon is highly unusual and previously unreported for opals. It cannot arise from polycrystallinity [24], because these structures are monodomain [see Figs. 2(a)-2(c)]. The size dispersion of the polymer spheres is not likely to influence the photonic properties since our size dispersions [25] are less than the reported onset values for such disorder scattering [26, 27]. In fact previous work has shown precisely the opposite response, with *no* scattered light escaping from inverted opals at the Bragg resonance in transmission [28].

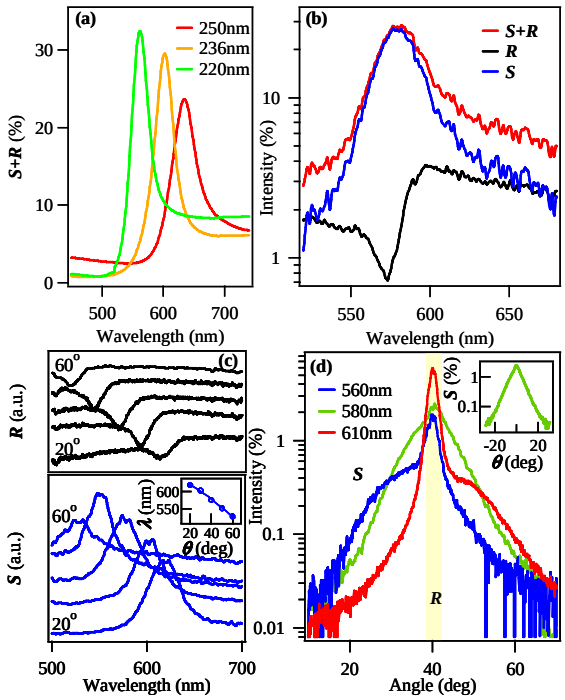

Fig. 5. (a). Evolution of the (111) bandgap for different sphere sizes at 5º incidence. (b) Scattering (*S*) and reflection (*R*) spectra for 40º incident angle. (c) Extracted *R*,*S* at different angles of incidence from 20º to 60º (in 10º steps), inset: fit to Bragg law. (d) Scattering with angle in the plane of incidence [horizontal cross-sections of Fig. 4(c)] around the specular reflected direction (at 40º) for selected colors around the bandgap. Inset: On-resonant scattering cross-section in orthogonal plane. (b-d) are taken for sample **S1**.

Angular cross-sections of the scattering cones [Fig. 5(d)] resolve the reflection and scattering components for different wavelengths around the bandgap (at 580nm for sample **S1**). The scattering cone passes across the specular reflection direction (which is the narrow peak shaded yellow) and is maximized at the Bragg condition [cf. Fig. 4(b)] while off-resonant wavelengths are scattered into directions depending on their spectral detuning from the band gap wavelength. Note these directions also change if the angle of incidence is changed, and are thus not fixed by the Bragg condition for escaping light. The width of the scattering cone reaches a maximum of 40º at the band gap. On the Bragg condition, the scattering falls off *exponentially* with angle [best seen in the orthogonal cross-section of the scattering cone taken perpendicularly to the incident plane, Fig. 5(d) inset] with no component of the specular reflection remaining (no angularly sharp component is observed). Fourier transforming this scattering dependence provides an estimate of the real-space scattering distribution, which has a long Lorentzian tail that implies that defects spatially localize light over length scales of many sphere periods.

#82645 - $15.00 USD Received 1 May 2007; revised 4 Jul 2007; accepted 9 Jul 2007; published 17 Jul 2007

The key to understanding these intriguing structural color properties are three important length scales: the typical penetration depth of resonant light inside the structure, known as the Bragg length, L_B; the scattering mean free path of photons between scattering events, l_{mfp}; and the absorption length of light, l_α. The Bragg length is controlled by the strength of reflection at each interface inside the material: the polymer opal has low refractive index contrast ($\Delta n/n$=0.06) leading to L_B~7μm while in high contrast TiO_2 inverse opals ($\Delta n/n$=1.18) L_B~1μm. On the other hand the scattering mean free path is controlled by scattering inside the imperfect structure, while the absorption length is almost 100 times this scattering length and easily measured from the non-resonant transmission through the sample [Fig. 6(a)].

Two different regimes are possible, shown schematically in Fig. 6. In an inverse opal [Fig. 6(b)], $L_B << l_{mfp}$, prohibiting backward scattering out of the crystal through two mechanisms. Firstly, resonant photons mostly reflect off the uppermost layers of the structure before scattering, while secondly when a non-resonant photon scatters internally into a resonant direction it is likely to be re-reflected into the structure. However, in these polymer opals [Fig. 6(c)] the opposite regime arises, $L_B \sim l_{mfp}$, which implies that all scattering events take place within the resonant photonic environment. We measure separately using coherent backscattering [Fig. 3(c)] that l_{mfp}~27μm off-resonance in the undoped material [see Fig. 6(a)], which decreases strongly on resonance. We note that the scattering mean free path is many times longer than the separation between doped nanoparticles, which have an estimated cross section of <5% due to their small size. Scattered photons are thus likely to escape the structure, while the enhanced optical density of states (ODoS) inside the photonic crystal resonantly enhances and redirects the scattering for particular wavelengths [Fig. 6(c)]. This process is highly sensitive to the size and location of the scatterers in the interstitial sites [29]. While the conventional ODoS integrates over 3D angles (as needed to calculate the radiative lifetime of an embedded emitter), the resonant scattering here is explicitly angle dependent and a different measure is required, the Mutual Density of States (MDOS) described in [30]. We surmise that essentially the scattering cross-section of defects inside such a low-contrast structure becomes large and anisotropic due to coupling with standing waves produced by multiple reflection. However, we note a full theoretical model has yet to be developed for this situation to describe the scattering enhancement from the angle-dependent local density of states - no current theoretical models incorporate 3D scattering and absorption within a photonic crystal environment. The scattering mean free path can be experimentally controlled by the level of doping [see Fig. 6(a)] and our current efforts include the characterization of the scattering induced by different nanoparticles. We note that since the sample thickness greatly exceeds l_{mfp}, different effects are observed in transmission [21]. Disorder effects in opals and colloidal crystals have recently become of increasing interest [31, 32] but have not observed the intense and angularly-broad scattering cones obtained here. Most work has been so far devoted to higher order bandgaps for which multiple scattering can become more important. Contrary to current efforts in obtaining complete bandgaps with *high index contrast* components, the previously unreported scattering-based structural color here requires *low* index contrast photonic crystals.

Finally, we show how doping the polymer opal with absorbing nanoparticles has such a dramatic effect on the scattering-based apparent color [Fig. 1(b-c)]. Angular scattering cross-sections for wavelengths around the resonant Bragg condition are measured for two opals with identical structures (samples **S3** and **S4,** bandgap at 570nm for 30º incidence) differing only in their nanoparticle doping levels [Figs. 6(d)-6(e)]. Again we confirm by TEM that such low loadings of small (<50nm) nanoparticle produces no obvious distortion of the periodic lattice [see Figs. 2(a)-2(b)]. Without absorbing nanoparticles (thin lines) the scattering is mostly diffuse, hence such samples (like most opals) look milky white with a faint color tinge strongly dependent on their orientation compared to light sources. With the absorbing nanoparticles selectively embedded in the interstices (thick lines), the resonant scattering increases and fills a much larger solid angle (note the overall diffuse light scattered from film also decreases). Examining the energy of light scattered into different directions [Fig. 6(e) shaded] shows that even 0.05% carbon nanoparticles loading increases the resonant scattering

#82645 - $15.00 USD Received 1 May 2007; revised 4 Jul 2007; accepted 9 Jul 2007; published 17 Jul 2007

by a factor of 300%, while the scattering cone width doubles. Hence these films appear strongly colored, virtually independent of illumination sources. Scattering inside such polymer opals can arise from Rayleigh scattering off the nanoparticle dopants or Mie scattering from lattice imperfections, and further experiments examining the anisotropy and polarization dependence (both weak) should help elucidate this.

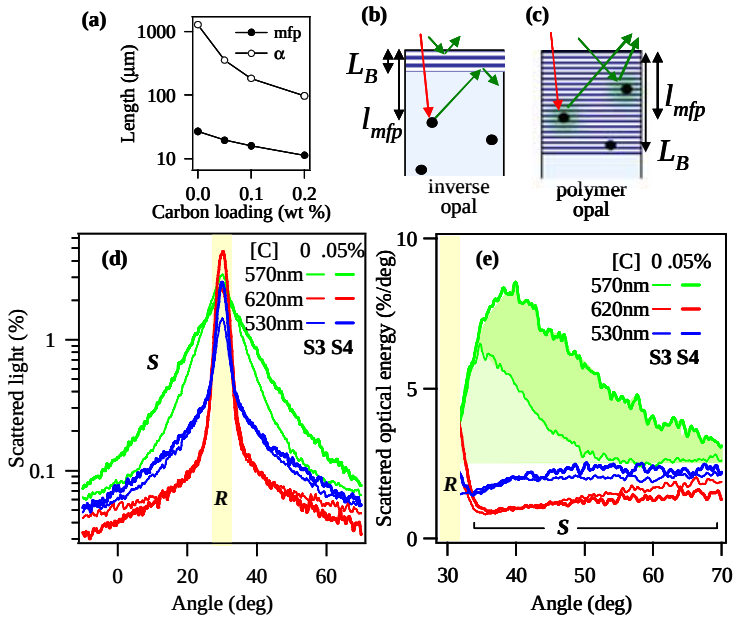

Fig. 6. (a). Effect of carbon loading on the scattering mean free path (l_{mfp}) and the absorption length (l_{α}), measured for samples **S3**-**6**. (b)-(c) Structural color formation schematically shown for (111) planes with black points representing scattering events (not nanoparticles). In an inverse opal (b), light incident at the Bragg angle (green) is directly reflected, while off-resonant light (red) that is scattered into this angle inside the structure cannot escape. In a polymer opal (c), all colors penetrate, and Bragg angle light is resonantly scattered. (d) Scattering cross-sections with angle for carbon nanoparticle doped (thick lines) and un-doped (thin lines) polymer opals at, and either side of, the bandgap at 570nm (samples **S3** & **S4**). (e) Scattered optical energy emerging in a 1° annulus around each angle for doped & undoped opals. Reflection (*R*) and scattering (*S*) domains indicated, resonant Bragg scattering shaded.

4. Conclusion

We have demonstrated experimentally that low-contrast polymeric photonic crystals exhibit radically different light scattering when doped interstitially at very low concentrations of carbon nanoparticles which both absorb and scatter light. Structural characterization shows this effect is not related to typical opaline disorder as the samples are similarly mono-domain with or without doping. We show that scattering is strongly enhanced in the Bragg condition, giving very wide viewing angles for the structural color. Such photonic crystals can be produced on an industrial scale (currently exceeding 1m x 100m sheets) and are easily tunable using different polystyrene precursor sizes and through nanoparticle doping. Hence the scope for spectrally-resonant scattering and enhanced structural color properties is extensive. Finally we believe such effects may also be widely found in nature.

Acknowledgments

This work was supported by EPSRC grant EP/C511786/1. OLJP acknowledges support of Merck KGaA and Helsingin Sanomat Centennial Foundation.

#82645 - $15.00 USD Received 1 May 2007; revised 4 Jul 2007; accepted 9 Jul 2007; published 17 Jul 2007